

Molecular Physics



An International Journal at the Interface Between Chemistry and Physics

ISSN: 0026-8976 (Print) 1362-3028 (Online) Journal homepage: https://www.tandfonline.com/loi/tmph20

Chemical activation of oxygen molecule by quantum electronic state selected vanadium cation: observation of spin-orbit state effects

Yih Chung Chang, Yuntao Xu, Bo Xiong & Cheuk-Yiu Ng

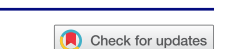
To cite this article: Yih Chung Chang, Yuntao Xu, Bo Xiong & Cheuk-Yiu Ng (2020): Chemical activation of oxygen molecule by quantum electronic state selected vanadium cation: observation of spin–orbit state effects, Molecular Physics, DOI: <u>10.1080/00268976.2020.1767309</u>

To link to this article: https://doi.org/10.1080/00268976.2020.1767309





DAVID PARKER FESTSCHRIFT



Chemical activation of oxygen molecule by quantum electronic state selected vanadium cation: observation of spin-orbit state effects

Yih Chung Chang , Yuntao Xu , Bo Xiong and Cheuk-Yiu Ng .

Department of Chemistry, University of California, Davis, CA, USA

ABSTRACT

By employing two-colour laser pulsed field ionisation-photoion (PFI-PI) double-quadrupole-double-octopole ion-molecule apparatus, we have examined the absolute integral cross-section (σ) for the reaction between vanadium cation (V⁺) and oxygen molecule (O₂), covering the centre-of-mass kinetic energy (E_{cm}) range of 0.2–10.0 eV. Here, V⁺ ion was prepared exclusively in its lowest 13 spin–orbit or J-states, $a^5D_{J=0-4}$, $a^5F_{J=1-5}$, and $a^3F_{J=2-4}$. The formation of VO⁺ + O is identified as the only product channel for these exothermic reactions. At $E_{cm}=0.2$ –5.0 eV, the σ values for the three electronic states are found to be in the order: $\sigma(a^3F_J) > \sigma(a^5D_J) > \sigma(a^5F_{JJ})$, whereas these cross-sections become nearly identical at $E_{cm}=5.0$ –10.0 eV. This observation has been rationalised by collision-mediated non-adiabatic electronic transitions. The J-state effect for the V⁺($a^3F_{2,3}$) + O₂ reactions are unambiguously identified for the first time for a reaction involving a transition metal cation. This J-state dependent chemical reactivity observed calls for rigorous theoretical interpretation. The fact that chemical reactivity for the a^5F_J excited state is lower than that for the a^5D_J ground state indicates that the difference in chemical reactivity is originated from quantum-electronic-state instead of energy effects.

• Conservation of total electron Spins • Weak Spin Crossing • J-state Effect on Reactivity $V^{+}(a^{3}F_{j}) + O_{2}(X^{3}\Sigma_{g}^{-})$ $V^{+}(a^{5}F_{j}) + O_{2}(X^{3}\Sigma_{g}^{-})$ $V^{+}(a^{5}D_{j}) + O_{2}(X^{3}\Sigma_{g}^{-})$ $V^{0^{+}}(x^{5}D_{j}) + O_{2}(X^{3}\Sigma_{g}^{-})$ $V^{0^{+}}(x^{5}D_{j}) + O_{2}(X^{3}\Sigma_{g}^{-})$ $V^{0^{+}}(x^{5}D_{j}) + O_{2}(x^{3}D_{j}) + O_{3}(x^{5}D_{j})$

ARTICLE HISTORY

Received 5 February 2020 Accepted 26 March 2020

KEYWORDS

Quantum state-selected vanadium cation; spin-orbit state effect on chemical reactivity

I. Introduction

Transition metal (TM) cations are known catalytic species for many homogeneous and inhomogeneous chemical reaction systems; and thus, the understanding of chemical reactivity for TM cations are important to many research fields that are of energy and environmental relevance [1,2]. In order to gain a global understanding of the bonding and catalytic properties of TM cations, it is necessary to perform detailed chemical reactivity studies of TM cations with a variety of representative molecules of different chemical classifications. The primary goal for the study of activation reactions, such as molecular oxygen (O_2) by a TM cation, is to learn about the reaction mechanism for efficient breaking

of the O-O bond to produce O atoms. In the presence of hydrocarbon species, highly reactive O atoms thus generated can lead to the formation of other reactive intermediates and chemical networks [3], which are valuable for the understanding of the chemistry involved in diverse research fields, such as astrochemistry, corrosion, catalysis, and atmospheric sciences [4].

As pointed out previously, the distinct electronic structures of TM cation species are resulted from interactions of valence electrons residing in partially filled and nearly degenerate ns and (n-1)d orbitals, where the principal quantum number n=4 and 5 are for 3d and 4d-TM cations, respectively. The dense manifolds of low-lying electronic states have also been shown to give rise to a

variety of electron spin multiplicities. Furthermore, due to the rigorous parity and electron spin selection rules, most low-lying electronic states of TM cations formed by photoionization of neutral precursors are metastable with long radiative lifetimes, which are significantly longer than the experimental cycle of about 100 μ s. The reactions of TM cation toward O_2 molecule have been extensively studied for 3d-TM cations (Sc⁺ – Zn⁺) [5–11], 4d-TM cations (Nb⁺, Ru⁺ – Ag⁺) [7,12,13], and 5d-TM cations (Lu⁺ – W⁺, Au⁺) [14,15].

As a model reaction involving TM cation, the reactivity of vanadium cation (V+) toward O2 has been investigated previously by measurements of reaction rate constants (k's) and absolute integral reaction cross sections (σ 's). The k measurements of the V⁺ + O₂ reaction obtained at room temperature using the Fourier transform ion-cyclotron and selected-ion flow tube methods [8,9] were reported by Koyanagi et al. By using a guided ion beam (GIB) ion-molecule reaction apparatus [5], Fisher *et al.* reported the σ 's for the same reaction in the centre-of-mass kinetic energy range of $E_{\rm cm} \approx$ 0.2–10.0 eV. These early studies of the $V^+ + O_2$ reaction were limited to reactions with reactant V⁺ ions prepared mostly in the a⁵D_I ground electronic state. Due to the difficulty of generating and identifying V⁺ ions in different excited electronic states [16], quantitative spin-orbit or J-state dependences of σ measurements for the $V^+ + O_2$ reaction have not been examined previously. Furthermore, the TM cation sources used previously were incapable of resolving spin-orbit J-states of V⁺ ion; and thus have prevented spin-orbit state selected σ measurements.

Recently, we have succeeded in developing a quantum electronic state selected ion source for TM cations, by which V⁺ cation can be prepared exclusively in a single of its lowest 13 spin-orbit states, a^5D_I (I = 0-4), a^5F_I (J = 1-5), and a^3F_I (J = 2-4), with high intensities and well-defined $E_{\rm cm}$ values [16]. By implementing this novel state-selected ion source based on two-colour laser pulsed field ionisation-photoion (PFI-PI) detection with the double-quadrupole-double-octopole (DQDO) ion-molecule reaction apparatus [17], we have successfully conducted σ measurements for the reactions of V⁺ ion towards CO₂ [18] and D₂ [19] as a function of not only $E_{\rm cm}$ but also spin-orbit J-state of V⁺ ion. In this paper, we present the results of a quantum spin-orbit electronic state selected study of the $V^+ + O_2$ reaction. The σ curves with V⁺ ions prepared in the $a^{5}D_{I}$ (J = 0-4), $a^{5}F_{I}$ (J = 1-4), and $a^{3}F_{J}$ (J = 2-3) states at $E_{\rm cm} = 0.2$ –10.0 eV have been obtained. In addition, J-state dependent reactivity measurements have been observed by comparing the reactivity of $V^+(a^3F_2)$ with that of V⁺(a³F₃) toward O₂. To our best knowledge.

This experiment represents the first observation of the spin–orbit J-state effect on chemical reactivity involving TM cations. We hope that this successful spin–orbit state selected σ measurement would motivate rigorous theoretical investigations to provide fundamental insight into how quantum electronic state, spin–orbit J-state, and electron spin of V⁺ cation promote or suppress chemical reactivity of the titled ion-molecule reactions.

II. Experimental considerations

The experimental arrangement and procedures of using the two-colour visible–ultraviolet (VIS-UV) laser PFI-PI DQDO ion-molecule apparatus have been described previously in detail. Briefly, the apparatus consists of two major components: namely, a two-colour VIS-UV laser PFI-PI ion source for quantum spin–orbit state selection [16], and a guided ion beam DQDO mass spectrometer for σ measurements of ion-molecule reactions [18,19]. A short description of the major features of these components are given below.

(a) Production of a gaseous supersonically cooled precursor V-atom beam: The gaseous neutral precursor V atoms were produced by laser ablation of a V rod employing the second harmonics output (532 nm, pulse energy = 2 mJ, repetition rate = 30 Hz) of a Nd:YAG laser. The V rod was driven by a stepping motor to translate and rotate. The plumes of plasma and neutral gaseous V species generated from laser ablation were cooled by collisions with a pulsed helium (He) gas flow in a capillary before supersonic expansion to form a supersonically cooled V/He seeded beam. The charged species thus produced in the V/He beam were removed by applying a DC deflection electric field right after the supersonic expansion. The V/He beam thus formed was skimmed by two conical skimmers before entering the laser photoexcitation (PEX) region.

(b) Two-colour VIS-UV laser PFI-PI V⁺ ion source: As pointed out previously, ion lenses E1, I1, and I2 are the most important elements of the ion source. The PEX region, defined by the space between ion lenses E1 and I1, is where the VIS-UV laser photoexcitation and the PFI-PI detection are conducted. One Nd:YAG laser (Spectra Physics Quanta-Ray PRO 290) operated at 30 Hz was used to pump two dye lasers simultaneously either by employing the 532 nm (second harmonics) or the 355 nm (third harmonics) outputs. The two independently tunable dye lasers yield the VIS ω_1 and UV ω_2 frequencies, which are merged by a dichroic mirror before propagating into the PEX centre, where the dye laser beams intersect the neutral V/He beam perpendicularly to generate V⁺ cation by means of the twocolour photoexcitation scheme. The VIS ω_1 frequency

is fixed at 21,841.4 cm⁻¹, which matches the transition frequency to the neutral excited state $V^*[3d^3(^4F) 4s4p]$ (${}^{3}P^{\circ}$), $z^{4}G^{\circ}_{5/2}$] from the neutral ground state V($3d^{3}4s^{2}$, $a^4F_{3/2}$) [20]. The fundamental output of the second dye laser is frequency doubled to generate UV ω_2 by passing the fundamental frequency through the BBO crystal as well as the beam path compensator. The UV ω_2 frequency is tuned in three frequency ranges of 32,438.5-32,918.6, 35,128.6–35,758.6, and 41,178.6–41,678.6 cm⁻¹, which can photoionize vanadium atom in the neutral excited state $V^*[3d^3(^4F)4s4p(^3P^\circ), z^4G^\circ_{5/2}]$ to generate V^+ cation in the a^5D_I (I = 0-4), a^5F_I (I = 1-5), and a^3F_I (J = 2-4) states, respectively.

A sequential electric field pulse scheme was conducted for PFI-PI detection in the PEX region after the twocolour laser photoexcitation. During the laser photoexcitation, the PEX region was maintained electric field free. Prompt V⁺ ions were produced by direct photoionization as well as autoionisation. A retarding electric field pulse, F_R (amplitude = 2.0–4.5 V/cm, duration = 2 μ s), was turned on at ion lens I1 at a delay of 150 ns measured with respect to the photoexcitation lasers. The F_R electric field pulse serves to retard prompt V⁺ ions towards the opposite direction of the neutral V-atom beam, resulting in spatial separation of prompt ions from high-n Rydberg $V^*(n)$ species that are populated by VIS-UV laser photoexcitation. Immediately following the ending of the $F_{\rm R}$ electric field pulse, the PFI electric field pulse, $F_{\rm PFI}$ (amplitude = 40 V/cm, duration = $0.7 \mu s$), was applied at ion lens E1. The F_{PFI} not only induces Stark-field ionisation of high-n Rydberg $V^*(n)$ species to generate PFI-PIs in selected quantum spin-orbit states, but also serves to extract PFI-PIs and prompt ions out of the ion source. We have pointed out previously that the key for achieving narrow kinetic energy spreads of the V⁺ PFI-PI beam is to turn off the F_{PFI} before V⁺ PFI-PIs pass through ion lens I1 such that all V⁺ PFI-PIs would gain the same momentum. Furthermore, the pulse nature of the F_R used makes prompt ions have lower kinetic energies compared to those of V⁺ PFI-PIs. Thus, a positive DC voltage applied at ion lens I2 can serve as an effective potential barrier to block off the prompt ions from exiting the ion source. As a result, only V⁺ PFI-PIs can surmount the DC voltage barrier to reach the reaction gas cell where ion-molecule reactions occur.

Readers are referred to the two-colour laser PFI-PI spectra for $V^+[a^5D_I (J = 0-4)], V^+[a^5F_I (J = 1-5)],$ and $V^{+}[a^{3}F_{I} (J = 2-4)]$ shown in Figures 8(a), 8(b), and 8(c) in Ref. [16], respectively. The J-state assignments are marked below the PFI-PI spectra for individual spin-orbit electronic states. The retarding and PFI electric field pulses used were given in individual figures. The IE values for the formation of all V⁺ spin-orbit states are known and are also given and marked by long droplines shown in these figures. The fully J-resolved PFI-PI spectra observed indicate that the preparation of V⁺ ion in single quantum spin-orbit electronic states is achieved.

(c) DODO ion-molecule reaction apparatus and σ measurements: The DQDO ion-molecule reaction apparatus consists of a reactant quadrupole mass filter (QMF), a dc quadrupole bender equipped with a microchannel plate (MCP) ion detector, an rf-octopole reaction gas cell, a product QMF and a Daly-type ion detector [17]. Thus, the DQDO apparatus can be considered as a fully inline QMS-ion guide-QMS instrument. Reactant V⁺ ions prepared in single spin-orbit states from the VIS-UV laser PFI-PI ion source are guided to enter reactant QMF, which is only used as an ion lens in this study. The MCP ion detector on top of the dc quadrupole bender is used for monitoring the ion transmission from the ion source up to the entrance of the reaction gas cell. The spin-orbit state selected V⁺ ions are injected into the rf-octopole reaction gas cell, where V⁺ ions react with O₂ molecules. Typically, O₂ pressure in the reaction gas cell is maintained at $\leq 2 \times 10^{-4}$ Torr. Product VO⁺ ions together with unreacted spin-orbit state selected V⁺ PFI-PI ions are collected and guided by the rf-octopole to enter the product QMF for mass analyses and ion intensity measurements. The ion TOF measurements were made by using a multichannel scalar.

In the present experiment, the laboratory kinetic energy (E_{lab}) carried by the V⁺ PFI-PI is converted to the $E_{\rm cm}$ by using the formula $E_{\rm cm} = E_{\rm lab} \, [{\rm M}/({\rm m}^+ + {\rm M})]$, where m⁺ and M represent the masses of the V⁺ ion and the O2 molecule, respectively. By changing the DC voltage applied to the rf-octopole relative to that for the PEX region of the PFI-PI ion source, the collision energy of the state selected V^+ PFI-PI ion can be varied in the E_{cm} range from 0.2 to 10.0 eV for collision energy dependent σ measurements. In this study, V⁺ ions in 11 of the 13 spin-orbit states, $V^{+}[a^{5}D_{I} (J = 0-4), a^{5}F_{I} (J = 1-4),$ and a^3F_I (I = 2, 3)], have been successfully chosen for $E_{\rm cm}$ dependence σ measurements.

III. Results and discussion

The main goal of the present experiment is to determine absolute integral cross sections for the formation of product VO⁺ ion from the V⁺(a^5D_I , a^5F_I , and a^3F_I) + O₂ reactions. However, the VO⁺ ion signal is found to have significant contributions of VO⁺ background ions originated from other sources. The analysis of TOF spectra for V⁺ and VO⁺ ions given below have allowed the identification and detection of the true VO⁺ product ion signal.

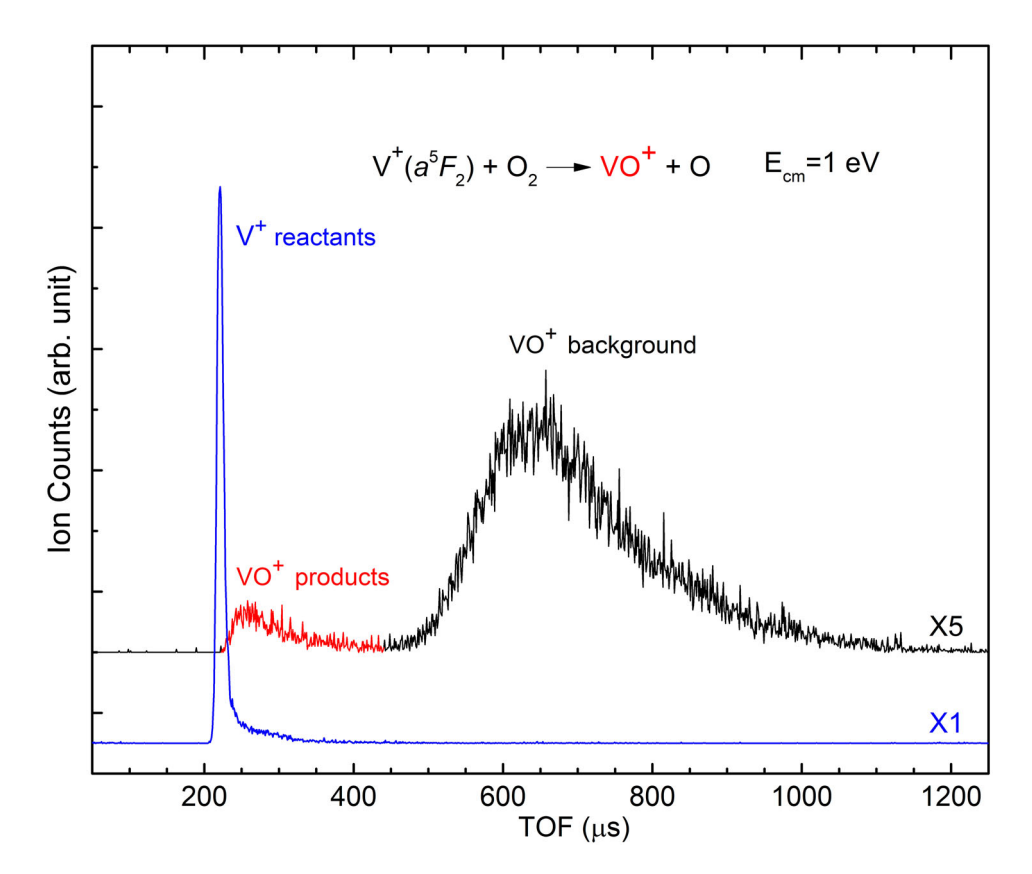


Figure 1. TOF spectrum for reactant V⁺ PFI-PIs in the a^5F_2 spin-orbit state (bottom blue curve) compared with the TOF spectrum for VO⁺ ions (top red-black curve). These TOF spectra for V⁺ and VO⁺ were recorded by setting $E_{cm} = 1.0$ eV for the V⁺ (a^5F_2) + O₂ reaction. In this measurement, the reaction gas cell was filled with O₂ gas at a pressure of 2×10^{-4} Torr. By comparing the TOF spectra for VO⁺ obtained with and without the F_{PFI} as shown below, the red (223-440 us) and black (440-1200 us) peaks of the TOF spectrum of VO⁺ have been identified as product and background VO⁺ ions, respectively. We note that the VO⁺ spectrum was magnified by a factor of five.

(a) TOF detection of V+ PFI-PI reactant and VO+ product ions: Figure 1 depicts the TOF spectra for reactant V⁺(a^5F_2) (bottom trace) and VO⁺ (top trace) obtained by setting the product QMF to select ion masses of 51 and 67 amu, respectively. In this measurement, the gas cell is filled with neutral O₂ gas at a pressure of 2×10^{-4} Torr. The reactant V⁺ ions observed are PFI-PI ions prepared in the V⁺(a^5F_2) spin–orbit state to react with O₂ in the rf-octopole reaction gas cell at $E_{\rm cm} = 1.0$ eV. The TOF peak for V⁺(a^5F_2) is identified as the intense and sharp ion peak centred at 220 µs. The TOF spectrum for VO⁺ exhibits two peaks with the weak one located at 223–440 µs (red trace), and the strong and broad one at 440–1200 µs (black trace).

As shown below, by comparing the TOF spectra observed under different experimental conditions, the nature of the TOF ion peaks can be obtained. A good indicator of observing a VO⁺ background ion peak is that the VO⁺ ion TOF peak remains unchanged when the PFI electric field pulse (F_{PFI}) or the photoexcitation lasers are turned off. We have identified that the VO⁺ ions

observed beyond 440 μ s (shown in black) are background ions; i.e. they are not produced from the V⁺ + O₂ reaction. Only the VO⁺ ions distributed in the 220–440 μ s TOF range (highlighted in red) are identified as VO⁺ product ions because these VO⁺ ions are observed when the F_{PFI} is turned on.

Taking the top spectrum of Figure 1 as the reference spectrum, we have placed this reference spectrum as the top spectrum in Figures 2 and 3, along with marking the contributions of VO⁺ product ions in red and background prompt ions in black. The middle spectrum (green trace) of Figure 2 was recorded under the same experimental conditions as that for the top spectrum except that no F_{PFI} pulse was applied. The bottom spectrum (blue trace) of Figure 2 is the TOF spectrum for VO⁺ background ions recorded when both the F_{PFI} pulse and the photoexcitation lasers are blocked. Since state selected $V^+(a^3F_2)$ PFI-PI ions cannot be generated without the F_{PFI} pulse or the laser photoexcitations, both the middle and bottom TOF spectra can be attributed to VO⁺ background ions. Furthermore, the comparison of Figure 2 confirms that the TOF peak in the range of

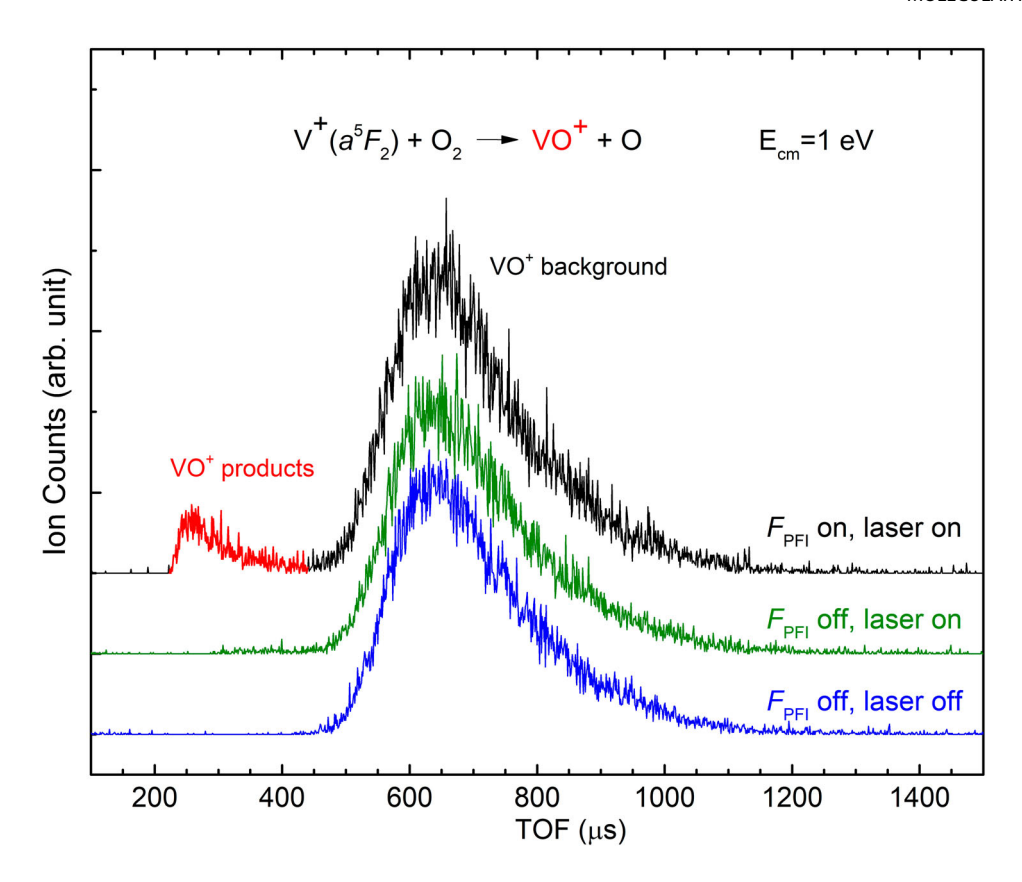


Figure 2. The top TOF spectra for VO⁺ of Figs. 1 and 2 are identical. The red TOF peak within 223–440 μ s in the top spectrum represents VO⁺ product from the V⁺(a⁵F₂) + O₂ reaction with $E_{cm} = 1$ eV, while the black peak beyond 440 μ s is assigned to VO⁺ background. The VO⁺ background assignment is verified by the middle green spectrum recorded when F_{PFI} electric field was off, and by the bottom blue spectrum recorded when both F_{PFI} electric field and photoexcitation laser was off.

220–440 μ s (highlighted in red) in the top TOF spectrum can be assigned as VO⁺ product ions formed by the V⁺(a^5F_2) + O₂ reaction.

Figure 3 compares the reference TOF spectrum for VO^+ recorded at $E_{cm} = 1.0 \, eV$ (top spectrum) with that obtained at $E_{\rm cm}=4.0\,{\rm eV}$ (middle spectrum). All other experimental conditions used for recording these spectra were the same as those used for recording the reference spectrum. The VO+ product ion peaks observed at 220-440 and 153-238 µs produced from the $V^+(a^5F_2) + O_2$ reaction at $E_{cm} = 1.0$ and 4.0 eV, are highlighted in red for the top and middle TOF spectra, respectively. This shift of the TOF peak for VO⁺ product ions towards shorter TOF range can be ascribed to the higher $E_{\rm cm}$ of 4.0 eV used in the TOF measurement. In the middle spectrum, another VO⁺ TOF peak situated in the range of 305 - 440 µs is also observed. This VO⁺ TOF peak is verified as a background ion peak based on its comparison with the bottom TOF spectrum, which was recorded without applying the F_{PFI} . The broad peak, that is not changed by PFI, electric field pulse, laser excitation, and/or E_{cm} setting, is believed to arise from chem-ionisation. The discussion on this rationalisation is given below.

Since the background VO⁺ ion intensity was found to depend on the application of the ablation laser and the filling of neutral reactant O₂ in the reaction gas cell, we believe that the major source of VO⁺ background is from chemi-ionisation reactions [21] between low-n Rydberg $V^*(n)$ and O_2 . During laser ablation of the V rod, energetic charged particles as well as excited neutral $V^*(n)$ species can be created. The charged particles were dispersed from the V/He beam by employing a DC deflection field of 400 V/cm applied downstream after the supersonic expansion. This DC deflection field can induce Stark-field ionisation of Rydberg $V^*(n)$, $n \ge 30$, species generated by the laser ablation source. These high-*n* Rydberg species lie in the region of $\approx 120 \, \mathrm{cm}^{-1}$ below the ionisation energy of V atom. Part of the low-n Rydberg $V^*(n)$, n < 30, species can have sufficiently long lifetimes to stay in the V/He beam and enter the reaction gas cell. For Rydberg $V^*(n)$ species, where $30 \ge n \ge 5$, the heat of formation at 0 K (ΔH_{f0}) of the $V^*(n) + O_2(X^3\Sigma_{g-})$ reactant state is greater than that of the product state $VO^+(X^3\Sigma^-) + O(^3P)$. Hence, it is energetically accessible to form $VO^+(X^3\Sigma^-)$ by chemiionisation reactions $V^*(30 \ge n \ge 5) + O_2(X^3\Sigma_g^-) \rightarrow$ $VO^+(X^3\Sigma^-) + O(^3P) + e^-$. Thus, these chemi-ionisation

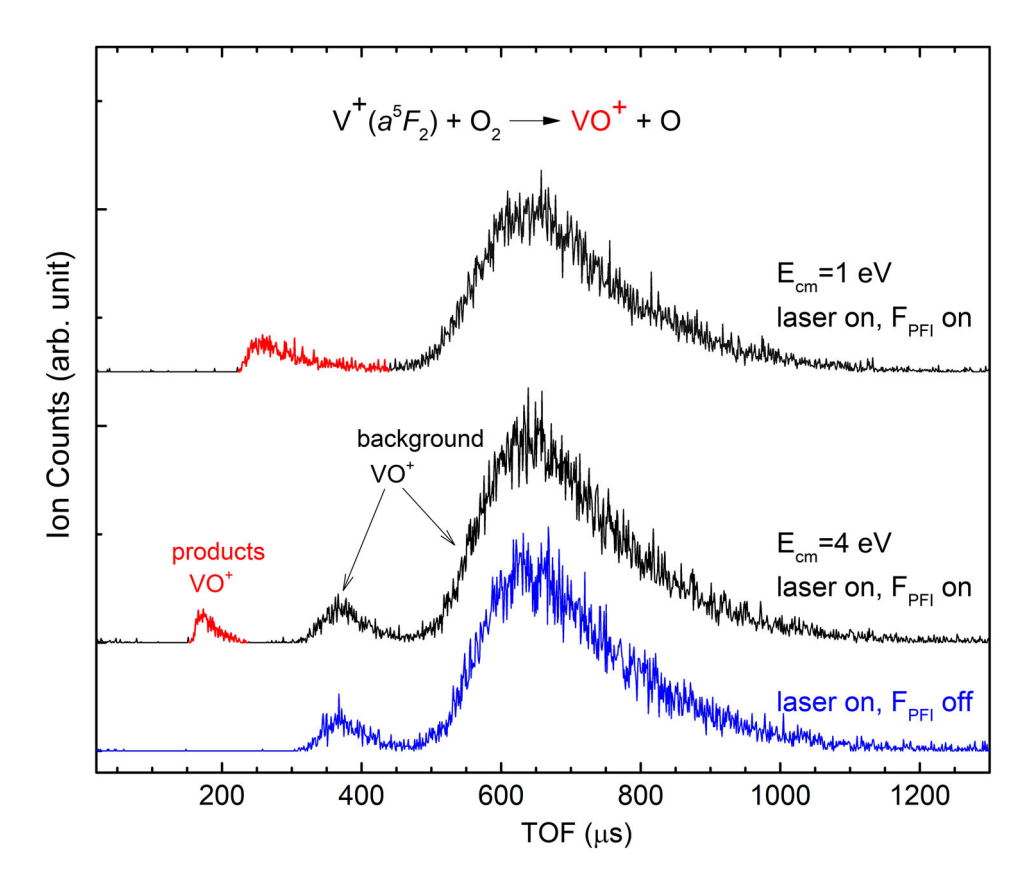


Figure 3. The red peaks shown both in top and middle spectra are verified to be VO⁺ product from the V⁺(a^5F_2) + O₂ reaction. The top and middle TOF spectrum was recorded when reaction collision energy was set as $E_{cm} = 1.0$ and 4.0 eV, respectively. The bottom spectrum was recorded under the same conditions as that of the middle spectrum except that the PFI electric field pulse F_{PFI} was turned off, aiming to verify the TOF ion peak observed at 310–466 μ s is a VO⁺ background peak.

reactions are most likely the major source of VO⁺ background ions observed in the present experiment.

Another source of VO⁺ background ions is believed to be originated from laser photoionization of neutral vanadium oxide (VO) formed by laser ablation of coated VO species on the surface of the V rod used, followed by laser photoionization. The VO⁺ background ion peak observed between 305 and 440 µs in the middle spectrum of Figure 3 is likely originated from this background source. At lower $E_{\rm cm} \leq 1$ eV, this weak VO⁺ background ion peak is expected to shift to a higher TOF region, resulting in strong overlap with the significantly broader and stronger VO⁺ background ion peak originated from chemi-ionisation reactions. Due to the weakness of the VO⁺ background ion peak arisen from laser photoionization of ablated VO, this background ion peak is indiscernible at $E_{\rm cm} = 1$ eV as shown in the top spectrum of Figure 3.

(b) Reactant and product states and heats of reaction: The heats of reaction (ΔE 's) for the reactions, $V^+(a^5D_J, a^5F_J, and <math>a^3F_{J)} + O_2(X^3\Sigma_g^-)$, leading to the formation of the $VO^+(X^3\Sigma_g^-) + O(^3P)$ product state are listed in

Reactions (1), (2), and (3), respectively.

$$V^{+}(a^{5}D_{0}) + O_{2}(X^{3}\Sigma_{g}^{-})$$

$$\rightarrow VO^{+}(X^{3}\Sigma^{-}) + O(^{3}P), \Delta E = -0.87 \pm 0.08eV$$

$$(1)$$

$$V^{+}(a^{5}F_{1}) + O_{2}(X^{3}\Sigma_{g}^{-})$$

$$\rightarrow VO^{+}(X^{3}\Sigma^{-}) + O(^{3}P), \Delta E = -1.20 \pm 0.08eV$$

$$(2)$$

$$V^{+}(a^{3}F_{2}) + O_{2}(X^{3}\Sigma_{g}^{-})$$

$$\rightarrow VO^{+}(X^{3}\Sigma^{-}) + O(^{3}P), \Delta E = -1.94 \pm 0.08eV$$

$$(3)$$

In Reaction (1), the ΔE value is obtained using available ΔH_{f0} values of all reactant and product species in their ground states [22,23]. The ΔE values for the electronically excited reactions (2) and (3) are obtained by taking into account of the corresponding known electronic energies of 0.3 and 1.1 eV for the a^5F_1 , and a^3F_2 electronic states measured with respect to the a^5D_0 ground electronic state of reactant V^+ ion [22]. The

 ΔE values of Reactions (1), (2), and (3) show that the V⁺($a^5\mathrm{D}_0$, $a^5\mathrm{F}_1$, and $a^3\mathrm{F}_2$) + O₂($X^3\Sigma_g^-$) reactions to form the VO⁺ + O product state in the ground state are all exothermic processes. In the discussion below, the absolute integral reaction cross sections for Reactions (1), (2), and (3) are designated as: $\sigma(a^5\mathrm{D}_0:\mathrm{VO}^+)$, $\sigma(a^5\mathrm{F}_1:\mathrm{VO}^+)$, and $\sigma(a^3\mathrm{F}_2:\mathrm{VO}^+)$, respectively.

(c) Quantum spin-orbit state effects on chemical reactivity of V^+ ion: We have examined not only the electronic state dependence, but also the spin-orbit Jstate effect on chemical reactivity within an electronic state of V^+ ion for the $V^+ + O_2$ reaction. Figure 4(a-c) depicts the σ curves for the formation of VO⁺ ion from the $V^+ + O_2$ reactions in the E_{cm} range of 0.2–10.0 eV with reactant V⁺ ion prepared exclusively in each of the J-states: (a) a^5D_I (I = 0-4); (b) a^5F_I (I = 1-4); and (c) $a^{3}F_{I}$ (I = 2-3). The $\sigma(a^{5}D_{0-4}: VO^{+}), \sigma(a^{5}F_{1-4}: VO^{+})$ and $\sigma(a^3F_{2-3}: VO^+)$ curves all show a monotonically decreasing trend as $E_{\rm cm}$ is increased, which is consistent with the exothermic nature of Reactions (1)–(3), and the prediction of the charge-induced dipole orbiting model. While the trends of the $\sigma(a^5D_I: VO^+)$ curves of this study and the previous GIB mass spectroscopic study [5] are in qualitative accord, the $\sigma(a^5D_1: VO^+)$ values obtained in the present experiment are found to be about twice as high as those reported previously. As pointed out previously, the purity of the $V^+(a^5D_0)$ ion source achieved in the present study is expected to be higher than that used in the latter GIB experiment.

The comparison of the $\sigma[a^5D_I (J = 0, 1, 2, 3, 4)$: VO⁺] curves of Figure 4(a) obtained in this study reveals no J-state dependences for the $\sigma(a^5D_{0-4}: VO^+)$, as these σ curves are nearly superimposable with each other after taking into account of the experimental uncertainties of $\pm 5\%$. The same observation was obtained for the $\sigma(a^5F_{1-4}: VO^+)$ curves as shown in Figure 4(b). Although both the $\sigma(a^5D_I: VO^+)$ and $\sigma(a^5F_I: VO^+)$ are found to be independent of J-state, the comparison of the $\sigma(a^3 F_2: VO^+)$ and $\sigma(a^3 F_3: VO^+)$ curves in the E_{cm} range of 0.2-10.0 eV clearly reveals the J-state effects. Interestingly, it is shown explicitly in Figure 4(c) that $\sigma(a^3F_2: VO^+) > \sigma(a^3F_3: VO^+)$ at $E_{cm} < 1.5 \text{ eV}$, while the reversed trend, $\sigma(a^3F_2: VO^+) < \sigma(a^3F_3: VO^+)$, is observed at $E_{\rm cm} > 1.5$ eV. The fact that the $\sigma(a^3F_2: VO^+)$ and $\sigma(a^3F_3: VO^+)$ measurements can be made simultaneously using only one laser dye has made possible the achievement of smaller uncertainties of 3-5% for the measurements of Figure 4(c). That is, the trends of the $\sigma(a^3F_2: VO^+)$ and $\sigma(a^3F_3: VO^+)$ curves depicted in Figure 4(c) are reliable. The $V^+(a^3F_3)$ state is 0.025 eV higher than the $V^+(a^3F_2)$ state. The higher chemical reactivity of $V^+(a^3F_2)$ toward O_2 than that of $V^+(a^3F_3)$ observed at $E_{\rm cm} < 1.5 \, {\rm eV}$ points to another example of

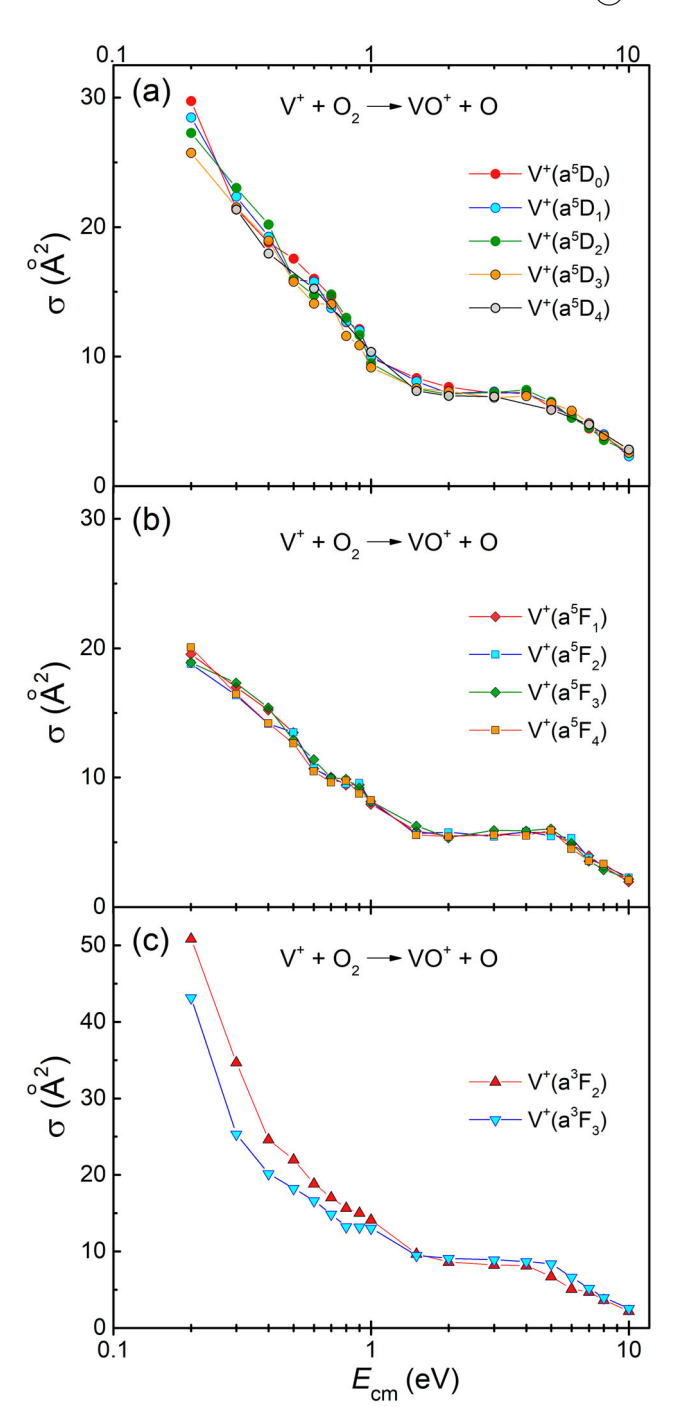


Figure 4. Absolute integral reaction cross sections for the V⁺ + O₂ \rightarrow VO⁺ + O reaction for reactant V⁺ ions prepared in (a) V⁺[a^5 D_J (J=0-4)] single spin–orbit states; (b) V⁺[a^5 F_J (J=1-4)] single spin–orbit states and (c) V⁺[a^3 F_J (J=2, 3)] single spin–orbit states. The σ curves are measured in the E_{cm} range of 0.2–10.0 eV.

quantum electronic state effect rather than energy effect for governing the chemical reactivity of V^+ ion.

As pointed out previously, the difference between the $\sigma(a^3F_2: VO^+)$ and $\sigma(a^3F_3: VO^+)$ curves is a reliable measure of the spin-orbit effect on chemical reactivity of the $V^+ + O_2$ reaction. Thus, this represents the first

observation of spin-orbit effect on chemical reactivity for an ion-molecule reaction involving a TM cation. Highlevel theoretical investigations are called for to provide a proper interpretation on chemical reactivity observed in the present study. Due to the low reactant $V^+(a^3F_4)$ ion intensities obtainable by the PFI-PI scheme, we have omitted the $\sigma(a^3F_4: VO^+)$ measurements in the present study. Nevertheless, the omission of these σ curves is not expected to alter the conclusion of this experiment. As expected, the comparison of Figure 4(c) shows that the J-state effect for chemical reactivity is more significant at lower $E_{\rm cm}$ values as the spin-orbit interaction energy becomes more important to influence the chemical process involved.

(d) Quantum electronic state effect on chemical reactivity: In order to look for quantum electronic state effects on chemical reactivity of reactant V⁺ prepared in different electronic states, V⁺(a³F_I, a⁵F_I, and a⁵D_I), we have compared in Figure 5 the $\sigma(a^3F_2: VO^+)$, $\sigma(a^5F_1: VO^+)$ VO⁺), and $\sigma(a^5D_0: VO^+)$ curves for Reactions (1)–(3), covering the $E_{\rm cm}$ range of 0.2–10.0 eV. At $E_{\rm cm} > 5.0$ eV, $\sigma(a^3F_2: VO^+)$, $\sigma(a^5F_1: VO^+)$, and $\sigma(a^5D_0: VO^+)$ are found to be nearly equal, whereas at $E_{\rm cm} \leq 5.0 \, {\rm eV}$, we find that $\sigma(a^3F_2: VO^+) > \sigma(a^5D_0: VO^+) > \sigma(a^5F_1:$ VO⁺), indicating that the reactant V⁺ ion in the triplet electronic state a³F₂ is more reactive than the quintet electronic states a⁵D₀ and a⁵F₁. Furthermore, the observed differences between $\sigma(a^3F_2: VO^+)$, $\sigma(a^5D_0:$ VO⁺), and $\sigma(a^5F_1: VO^+)$ appear to increase as E_{cm} is decreased. At sufficiently low E_{cm} values, we expect the spin-orbit interaction to play a more significant role in determining the chemical reactivity of V⁺ ion. Since these electronic states are metastable and have long lifetimes, they do not communicate well with each other. Thus, chemical reactivity of V^+ observed at low E_{cm} is expected to be determined by individual electronic states.

The Bonn-Oppenheimer approximation only allows the reaction to propagate and take place in single potential energy surfaces, and thus, the transition to other potential energy surfaces necessarily induced by nonadiabatic couplings [24–26]. Previous experiments have shown efficient conversion of electronic energy to kinetic energy. Thus, the communication between different electronic states of V⁺ ion can be achieved by collisionmediated non-adiabatic transitions. The dispersion and mixing of nearby electronic states resulted from nonadiabatic interactions can give rise to an averaging effect on chemical reactivity, yielding similar $\sigma(a^3F_2: VO^+)$, $\sigma(a^5D_0: VO^+)$, and $\sigma(a^5F_1: VO^+)$ values at higher E_{cm} values as shown in Figure 5. Since this and recent similar experiments on chemical reactivity studies can involve many electronic states, the ability illustrated here for

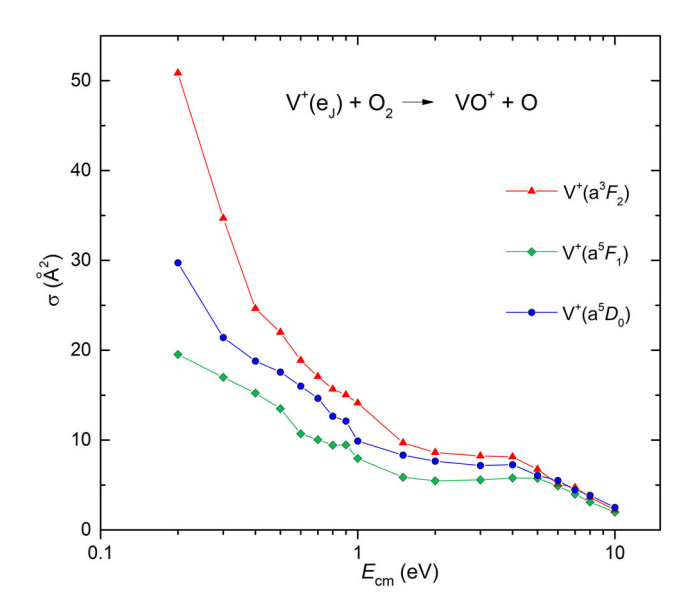


Figure 5. Comparison of absolute integral reaction cross sections, $\sigma(a^5D_0:VO^+)$, $\sigma(a^5F_1:VO^+)$, and $\sigma(a^3F_2:VO^+)$. All σ curves are measured in the $E_{\rm cm}$ range of 0.2–10.0 eV.

probing chemical reactivity of individual electronic states should make these experiments attractive for the study of non-adiabatic effects on chemical dynamics.

(e) Schematic energy level diagram for the $V^+ + O_2$ reaction system: To facilitate the discussion concerning the reaction mechanism for activation of O2 molecule by V⁺ ion, we show in Figure 6 a simplified schematic energy level diagram for the $V^+ + O_2$ reaction system in the heat of formation scale.

Here, the three reactant states: $V^+(a^3F_2) + O_2(X^3$ $\Sigma_{\rm g}^{-}$), V⁺(a⁵F₁) + O₂(X³ $\Sigma_{\rm g}^{-}$), and V⁺(a⁵D₀) + O₂(X³ $\Sigma_{\rm g}^{-}$), are listed on the left column and the product states on the right column of the figure. Since the dominant product channel for the $V^+ + O_2$ reaction system is $VO^+ + O$, and the energetics for the $VO^+(X^3\Sigma^-, A^3\Delta, B^3\Phi)$, and $C^3\Pi$) electronic states are known [27,28], we have included the excited product states, $VO^+(A^3\Delta) + O(^3P)$, $VO^+(B^3\Phi) + O(^3P)$, and $VO^+(C^3\Pi) + O(^3P)$ in the energy level diagram, in addition to the $VO^+(X^3\Sigma^-) + O(^3P)$ ground product state. The calculated energy levels and symmetry designations of the five lowest surmised intermediates are shown in the middle column of the energy level diagram. The arrow on the bottom of Figure 6 shows the direction of the reaction coordinate.

For the $V^+(a^3F_2) + O_2(X^3\Sigma_g^-)$ reactant state and the $VO^{+}(X^{3}\Sigma^{-}) + O(^{3}P), VO^{+}(A^{3}\Delta) + O(^{3}P), VO^{+}(B^{3}\Phi)$ $+ O(^{3}P)$ and $VO^{+}(C^{3}\Pi) + O(^{3}P)$ product states, the total electron spin angular momenta can be S = 2, 1, and 0; and thus the corresponding (2S + 1) spin multiplicities of individual reactant and product states can be 5 (quintet), 3 (triplet), and 1 (singlet). Since the

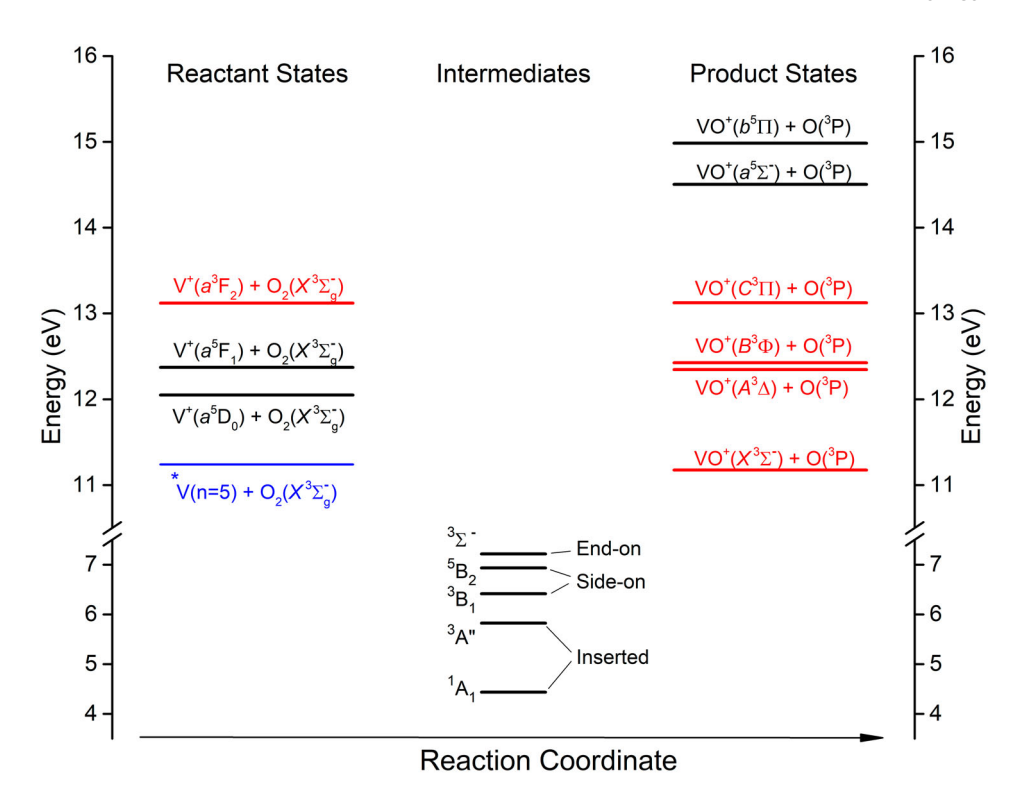


Figure 6. Schematic energy level diagram of the $V^+ + O_2$ reaction system in the heat of formation scale. The reactant states, $V^+(a^5D_0) + O_2$ (black line), $V^+(a^5F_1) + O_2$ (black line), and $V^+(a^3F_2) + O_2$ (red line) are shown on the left; the intermediates based on previous theoretical calculations are shown in the middle of the figure. Possible products channels are depicted on the right side highlighted in red, black, based on their multiplicities. The reactant state of $V^*(n=5) + O_2(X^3\Sigma_q^-)$ is highlighted by blue.

 $V^+(a^3F_2) + O_2(X^3\Sigma_g^-)$ reactant state and the ground $VO^+(X^3\Sigma^-) + O(^3P)$ product state have the same singlet, triplet, and quintet multiplicities, they are 100% correlated, fulfilling the total electron spin conservation rule and thus giving rise to high chemical reactivity for Reaction (3). Following the same colour code as that adopted in previous studies, the fully correlated $V^+(a^3F_2) + O_2(X^3\Sigma_g^-)$ reactant state and the $VO^{+}(X^{3}\Sigma^{-}) + O(^{3}P), VO^{+}(A^{3}\Delta) + O(^{3}P), VO^{+}(B^{3}\Phi)$ $+ O(^{3}P)$ and $VO^{+}(C^{3}\Pi) + O(^{3}P)$ product states are highlighted in red. Furthermore, the fully correlated $V^{+}(a^{5}F_{J}) + O_{2}(X^{3}\Sigma_{g}^{-})$ and $V^{+}(a^{5}D_{J}) + O_{2}(X^{3}\Sigma_{g}^{-})$ reactant states and the excited $VO^+(a^5) + O(^3P)$ and $VO^+(b^5) + O(^3P)$ product states are highlighted in black.

As shown in Figure 6, the five lowest intermediate states are predicted to have the symmetry designations of (1A1, 3A") for the inserted VO2+ structure; (3B₁, 5B₂) for the side-on (V-O₂)⁺ structure; and ${}^{3}\Sigma^{-}$ for the end-on (V-O-O)⁺ structure [8] According to the electron spin conservation rule, these five calculated intermediates can fully couple with the $V^+(a^3F_2) + O_2(X^3\Sigma_g^-)$ reactant state, leading to the formation of the $VO^+(X^3\Sigma^-) + O(^3P)$, $VO^{+}(A^{3}\Delta) + O(^{3}P), VO^{+}(B^{3}\Phi) + O(^{3}P) \text{ and } VO^{+}(C^{3})$ Π) + O(³P) product states. That is, the formation of the ground product state $VO^+(X^3\Sigma^-) + O(^3P)$ from the $V^{+}(a^{3}F_{2}) + O_{2}(X^{3}\Sigma_{g}^{-})$ reactant state can be achieved with additional correlation or mediation via the lowest singlet, triplet, and quintet ¹A₁, ³A", ³B₁, ⁵B₂, and ${}^3\Sigma^-$ intermediate states. Furthermore, it is also energetic allowed for the $V^+(a^3F_2) + O_2(X^3\Sigma_g^-)$ reactant state to form product states, $VO^+(X^3\Sigma^-) + O(^3P)$, $VO^{+}(A^{3}\Delta) + O(^{3}P), VO^{+}(B^{3}\Phi) + O(^{3}P) \text{ and } VO^{+}$ $(C^3\Pi) + O(^3P)$.

The electron configuration of $V^+(a^5F_1)$ is $(3d)^3(4s)^1$ is same as that of $V^+(a^3F_I)$ except that the total electron spin is 2 for the quintet state and 1 for the triplet state. For the reactant state, $V^+(a^5F_I) + O_2(X^3\Sigma_g^-)$, the total electron spin can be S = 3, 2, and 1 with the corresponding (2S+1) multiplicaties to be 7 (septet), 5 (quintet), and 3 (triplet). Thus, only the quintet and triplet multiplicities of the $V^+(a^5F_J) + O_2~(X^3\Sigma_g^-)$ reactant states can directly correlate to the $VO^+(X^3\Sigma^-) + O(^3P)$ product state via mediation by the triplet and quintet ${}^{3}A''$, ${}^{3}B_{1}$, 5B_2 , $^3\Sigma^-$ intermediates. The V⁺(a^5F_J) + O₂($X^3\Sigma_g^-$) and $V^+(a^5D_J) + O_2 (X^3\Sigma_g^-)$ reactant states with septet multiplicity should lead to septet intermediates resulting in septet multiplicity product states, such as the excited $VO^{+}(a^{5}\Sigma^{-}) + O(^{3}P)$ and $VO^{+}(b^{5}\Pi) + O(^{3}P)$ product states, which is also included in the energy diagram of Figure 6. Assuming the Wigner-Witmer spin-conservation rule to be valid [18,29], the 'weak spin-crossings' between septet to quintet, as well as triplet to singlet reaction surfaces are expected to hold. The above analysis based on the total electron spin conservation indicates that out of the septet, quintet, and triplet multiplicities for the $V^+(a^5F_1) + O_2(X^3\Sigma_g^-)$ reactant state, only the quintet and triplet multiplicities can directly correlate to the $VO^+(X^3\Sigma^-) + O(^3P)$ ground product state. Thus, the probability for the $V^{+}(a^{5}F_{I}) + O_{2}(X^{3}\Sigma_{g}^{-})$ reactant state to be in quintet and triplet multiplicities is $(3+5)/(3+5+7) \approx 53\%$, suggesting that the $V^+(a^3F_2) + O_2 (X^3\Sigma_g^-)$ reactant state could be up to a factor of two more reactive than the V⁺(a^5F_1) + $O_2(X^3\Sigma_g^-)$ reactant state. Due to the high endothermicity to form the $VO^+(a^5\Sigma^-) + O(^3P)$ and $VO^+(b^5\Pi) + O(^3P)$ product states, the septet multiplicity of the V⁺(a^5F_1) + O₂ ($X^3\Sigma_g^-$) reactant state is expected to be less reactive. Nevertheless, the observation that the $\sigma(a^5F_1: VO^+)$ is $\approx 40-60\%$ of the $\sigma(a^3 F_2: VO^+)$ at $E_{cm} < 4.0 \, eV$, as shown in Figure 5, seems to be in accord with the rationalisation presented above based on the total electron spin conservation

As shown in Figure 5, $V^+(a^5F_I)$ ion exhibits the lowest chemical reactivity toward $O_2(X^3\Sigma_g^-)$, even though its electronic energy is about 0.3 eV higher than that of the $V^+(a^5D_0)$ ground state. The electron spin multiplicities of the V⁺(a^5F_I) + O₂ ($X^3\Sigma_g^-$) reactant state are the same as that of the ground reactant state, therefore the reaction can lead to the ground product state via the intermediates of the ${}^3A''$, 3B_1 , 5B_2 , and ${}^3\Sigma^-$ symmetry. The electronic configuration for $V^+(a^5D_0)$ is $(3d)^4$ and for $V^+(a^5F_1)$ is $(3d)^3(4s)^1$. It has been suggested that a valence electron in 4s orbital might cause lower reactivity of $V^+(a^5F_1)$, as the electron filled in 4s orbital may make $V^+(a^5F_1)$ more repulsive than $V^+(a^5D_0)$ when O_2 approaches V^+ [30,31]. The observation of lower reactivity of $V^+(a^5F_I)$ than that of $V^+(a^5D_I)$ indicates that it is not an energy effect, but a quantum electronic effect in determining chemical reactivity of V⁺ ion.

IV. Conclusion and summary

By coupling a novel quantum spin-orbit state selected TM ion source with the DQDO ion-molecule reaction apparatus developed in our laboratory, we have conducted a detailed integral cross section measurement for the $V^+ + O_2 \rightarrow VO^+ + O$ reaction covering the collision energy range of $E_{\rm cm} = 0.2 - 10.0 \, {\rm eV}$. Here, reactant V⁺ ions were prepared in 11 quantum spin-orbit J-states: a^5D_I (I = 0-4), a^5F_I (I = 1-4), and a^3F_I (I = 2-3). Spin-orbit J-state effect on chemical reactivity of the

 $V^{+}(a^{3}F_{2,3}) + O_{2}$ reactions are observed for the first time for ion-molecule reactions involving TM cations. Although no explicit J-state dependent chemical reactivity measurements are found for reactant V⁺ ion prepared in the a^5D_I and a^5F_I electronic states, the J=2 and 3 states for the $V^+(a^3F_I)$ excited electronic states are shown to have different chemical reactivity toward O₂ molecule. It is shown explicitly that $\sigma(a^3F_2: VO^+) > \sigma(a^3F_3: VO^+)$ at $E_{\rm cm} < 1.5 \, {\rm eV}$, while the trend becomes $\sigma({\rm a}^3 {\rm F}_2: {\rm VO}^+)$ $< \sigma(a^3F_3: VO^+)$ at $E_{cm} > 1.5$ eV. The observation of higher reactivity of $V^+(a^3F_I)$ ion than that of $V^+(a^5F_I)$ and $V^+(a^5D_I)$ ions toward $O_2(X^3\Sigma_g^-)$ is consistent with the total electron spin conservation reaction mechanism. High-level theoretical investigations are called for the interpretation of spin-orbit effect on chemical reactivity observed in the present study.

Acknowledgements

This material is based upon work supported by the National Science Foundation under CHE-1763319. CYN is also grateful to Dr Huie Tarng Liou for his generous donation of research support for the Ng Laboratory.

Disclosure statement

No potential conflict of interest was reported by the author(s).

Funding

This material is based upon work supported by the National Science Foundation [grant number CHE-1763319].

ORCID

Yih Chung Chang http://orcid.org/0000-0002-3763-1864 Yuntao Xu 🗅 http://orcid.org/0000-0002-1205-8168 Bo Xiong http://orcid.org/0000-0002-8985-6897 Cheuk-Yiu Ng http://orcid.org/0000-0003-4425-5307

References

- [1] D.K. Böhme and H. Schwarz, Angew. Chem. Int. Ed. 44 (16), 2336-2354 (2005).
- [2] E. Harris, B. Sinha, D. van Pinxteren, A. Tilgner, K.W. Fomba, J. Schneider, A. Roth, T. Gnauk, B. Fahlbusch and S. Mertes, Science. 340 (6133), 727-730 (2013).
- [3] P. Armentrout and J. Beauchamp, Acc. Chem. Res. 22 (9), 315-321 (1989).
- [4] E. Murad, J. Geophys. Res. Space Phys. 83 (A12), 5525-5530 (1978).
- [5] E.R. Fisher, J. Elkind, D. Clemmer, R. Georgiadis, S. Loh, N. Aristov, L. Sunderlin and P.B. Armentrout, J. Chem. Phys. 93 (4), 2676-2691 (1990).
- [6] M. Rodgers, B. Walker and P. Armentrout, Int. J. Mass Spectrom. 182, 99-120 (1999).
- S. Loh, L. Lian and P. Armentrout, J. Chem. Phys. 91 (10), 6148-6163 (1989).



- [8] G.K. Koyanagi, D.K. Bohme, I. Kretzschmar, D. Schröder and H. Schwarz, J. Phys. Chem. A. 105 (17), 4259-4271
- [9] G.K. Koyanagi, D. Caraiman, V. Blagojevic and D.K. Bohme, J. Phys. Chem. A. 106 (18), 4581-4590 (2002).
- [10] P. Armentrout, L. Halle and J. Beauchamp, J. Chem. Phys. 76 (5), 2449-2457 (1982).
- [11] S. Loh, E.R. Fisher, L. Lian, R.H. Schultz and P. Armentrout, J. Phys. Chem. 93 (8), 3159-3167 (1989).
- [12] Y.M. Chen and P. Armentrout, J. Chem. Phys. 103 (2), 618-625 (1995).
- [13] X.-G. Zhang and P. Armentrout, J. Phys. Chem. A. 107 (42), 8904-8914 (2003).
- [14] F.-X. Li, K. Gorham and P. Armentrout, J. Phys. Chem. A. **114** (42), 11043–11052 (2010).
- [15] Y. Matsuo, H. Maeda and M. Takami, Chem. Phys. Lett. 201 (1-4), 341-344 (1993).
- [16] Y.-C. Chang, B. Xiong, Y. Xu and C.-Y. Ng, J. Phys. Chem. A. 123 (12), 2310-2319 (2019).
- [17] Y.C. Chang, Y. Xu, Z. Lu, H. Xu and C. Ng. J. Chem. Phys. 137 (10), 104202 (2012).
- [18] Y.C. Chang, Y. Xu and C.-Y. Ng, Phys. Chem. Chem. Phys. 21, 6868-6877 (2019).
- [19] Y. Xu, Y.-C. Chang and C.-Y. Ng, J. Phys. Chem. A. 123 (28), 5937-5944 (2019).

- [20] A. Kramida, Y. Ralchenko, J. Reader and NIST ASD Team. NIST Atomic Spectra Database (ver. 5.6.1). (National Institute of Standards and Technology, 2018). https://doi.org/10.18434/T4W30F.
- [21] M. Gress, S. Linn, Y. Ono, H. Prest and C. Ng,, J. Chem. Phys. 72 (7), 4242-4244 (1980).
- [22] S.L. Bennett, S.-S. Lin and P.W. Gilles, J. Chem. Phys. 78 (3), 266-273 (1974).
- [23] G. Balducci, G. Gigli and M. Guido, J. Chem. Phys. 79 (11), 5616-5622 (1983).
- [24] J.C. Tully, J. Chem. Phys. **93** (2), 1061–1071 (1990).
- [25] J.C. Tully, J. Chem. Phys. 137 (22), 22A (2012). 301.
- [26] J.C. Tully and R.K. Preston, J. Chem. Phys. 55 (2), 562–572 (1971).
- [27] J.M. Dyke, B.W.J. Gravenor, M.P. Hastings and A. Morris, J. Phys. Chem. **89** (21), 4613–4617 (1985).
- [28] Luo, Z.; Chang, Y. C.; Lam, C. S.; Lau, K. C.; Ng, C. Y., in Frontiers and Advances in Molecular Spectroscopy, edited by J. Laane (Elsevier, 2018), pp. 195-249.
- [29] H. Schwarz, Int. J. Mass Spectrom. 237 (1), 75-105 (2004).
- [30] J. Elkind and P. Armentrout, J. Phys. Chem. 91 (8), 2037-2045 (1987).
- [31] J.C. Weisshaar, Acc. Chem. Res. 26 (4), 213-219 (1993).